recording electrodes were filled with a solution containing (in mM) 120 K-gluconate, 20 KCl, 10 Hepes, 1 EGTA, 1.3 $MgCl_2$, 0.1 $CaCl_2$, 2 Mg-ATP, 0.3 GTP, and 0.1 leupeptin. All recordings were obtained in the presence of 10 μM bicuculline. Miniature EPSCs obtained in the presence of tetrodotoxin (0.5 μM) were stored on videotape and analyzed off-line. Data were compared statistically with the nonparametric Kolmogorov-Smirnov test or the paired Student's *t* test. Significance was assessed at $P < 0.05$. All data are reported as the mean ± SEM.

13. PPF is expressed as the amplitude ratio (S2/S1) of the second synaptic response (S2) over the first synaptic response (S1).
14. M. Scanziani, P. A. Salin, K. E. Vogt, R. C. Malenka, R. A. Nicoll, *Nature* **385**, 630 (1997).
15. M.-Y. Min, D. A. Rusakov, D. M. Kullmann, *Neuron* **21**, 561 (1998).
16. L. A. Schrader, J. G. Tasker, *J. Neurophysiol.* **77**, 527 (1997).
17. G. Tong, C. E. Jahr, *Neuron* **13**, 1195 (1994).
18. J. S. Diamond, C. E. Jahr, *J. Neurosci.* **71**, 4672 (1997).
19. G. Liu, S. Choi, R. W. Tsien, *Neuron* **22**, 395 (1999).
20. A. B. Brussaard *et al.*, *Neuron* **19**, 1103 (1997).
21. D. A. Poulain, J. B. Wakerley, *Neuroscience* **7**, 773 (1982).
22. P. Jourdain *et al.*, *J. Neurosci.* **18**, 6641 (1999).
23. J. S. Isaacson, *Neuron* **23**, 377 (1999).
24. V. Gallo, C. A. Ghiani, *Trends Pharmacol. Sci.* **21**, 252 (2000).
25. P. R. Laming *et al.*, *Neurosci. Biobehav. Rev.* **24**, 295 (2000).
26. L. M. Garcia-Segura, F. Naftolin, J. B. Hutchison, I. Azcoitia, J. A. Chowen, *J. Neurobiol.* **40**, 474 (1999).
27. J. A. Mong, M. M. McCarthy, *J. Neurobiol.* **40**, 602 (1999).
28. S. H. R. Oliet, D. A. Poulain, *J. Physiol.* **520**, 815 (1999).
29. We thank D. T. Theodosis for helpful discussions and comments on the manuscript. Supported in part by grants from the Conseil Régional d'Aquitaine (970301209) and from the Association pour la Recherche Médicale en Aquitaine. R.P. is supported by the French Ministry of Education.

19 January 2001; accepted 8 March 2001

Glia-Synapse Interaction Through Ca^{2+}-Permeable AMPA Receptors in Bergmann Glia

Masae Iino,[1,2] Kaori Goto,[1,2] Wataru Kakegawa,[1,2] Haruo Okado,[2,3] Makoto Sudo,[1] Shogo Ishiuchi,[1,2] Akiko Miwa,[2,3] Yukihiro Takayasu,[1,2] Izumu Saito,[4] Keisuke Tsuzuki,[1,2] Seiji Ozawa[1,2]*

Glial cells express a variety of neurotransmitter receptors. Notably, Bergmann glial cells in the cerebellum have Ca^{2+}-permeable α-amino-3-hydroxy-5-methyl-4-isoxazolepropionic acid (AMPA)–type glutamate receptors (AMPARs) assembled without the GluR2 subunit. To elucidate the role of these Ca^{2+}-permeable AMPARs, we converted them into Ca^{2+}-impermeable receptors by adenoviral-mediated delivery of the GluR2 gene. This conversion retracted the glial processes ensheathing synapses on Purkinje cell dendritic spines and retarded the removal of synaptically released glutamate. Furthermore, it caused multiple innervation of Purkinje cells by the climbing fibers. Thus, the glial Ca^{2+}-permeable AMPARs are indispensable for proper structural and functional relations between Bergmann glia and glutamatergic synapses.

AMPARs are expressed ubiquitously in both neurons and glial cells (*1–3*). Although they are known to mediate fast excitatory synaptic transmission in most brain neurons, their function in glia is uncertain. AMPARs are assembled from the four subunits, GluR1 through GluR4, either alone or in various combinations. The functional properties of AMPARs depend on their subunit composition: AMPARs possessing the GluR2 subunit exhibit either a linear or outwardly rectifying current-voltage (*I-V*) relation and little Ca^{2+} permeability, whereas receptors lacking GluR2 show strong inward rectification and high Ca^{2+} permeability (*4, 5*). In Bergmann glia, only GluR1 and GluR4 mRNAs are expressed; therefore, their AMPARs exhibit inward rectification and are highly permeable to Ca^{2+} (*6–8*).

To elucidate the functional role of the Ca^{2+} permeability of AMPARs in Bergmann glia, we attempted to convert Ca^{2+}-permeable AMPARs into Ca^{2+}-impermeable receptors by adenoviral-mediated delivery of the GluR2 gene. We constructed two recombinant adenoviruses: one for expression of Cre recombinase (AxCANCre) and another bearing a switching unit that consisted of the CAG promoter, a stuffer flanked by a pair of *loxP* sites, and GluR2 cDNA (AxCALNLGluR2) (*9*). We injected these two recombinant adenoviruses together with the recombinant adenovirus bearing green fluorescent protein (GFP) cDNA (AxCAGFP) into the molecular layer of the cerebellar cortex of 20- to 24-day-old rats. Because the adenovirus has much higher affinity to glial cells than neurons, expression of both GFP and GluR2 was detected predominantly in Bergmann glia in the infected areas 2 days after inoculation (Fig. 1, A through C) (*9*). The number of plaque-forming units (PFU) of AxCAGFP in the viral mixture for injection was adjusted to 1/4 to 1/40 the number of PFU of AxCALNL-GluR2 so expression of GluR2 was detected in almost all Bergmann glial cells emitting GFP fluorescence. GFP and GluR2 were detected simultaneously, even when they were expressed in single isolated glia (Fig. 1, D through F). In some experiments, we coexpressed GluR2 and GFP in Bergmann glia using a recombinant adenovirus bearing GluR2 cDNA, the internal ribosomal entry site (IRES) sequence, and GFP cDNA (AxCALALGluR2-IRES-GFP) (*9*). In Bergmann glia infected with this recombinant virus together with AxCAN-Cre, we also detected simultaneous expression of GFP and GluR2.

We next examined the effects of GluR2 expression on the electrophysiological properties of AMPARs in Bergmann glial cells (*9*). We recorded current responses to the iontophoretic application of AMPA in the presence of 50 μM cyclothiazide (CTZ), which reduces desensitization of AMPARs (*10–12*) (Fig. 2). In Bergmann glia without expression of GluR2 in slices infected with AxCALNLGluR2 and AxCAGFP but without AxCANCre, the *I-V* relation invariably exhibited strong inward rectification. The permeability to Ca^{2+} of AMPARs was examined by substituting Na^+-free, 10 mM Ca^{2+} solution for normal saline (*13*). AMPA elicited inward currents at potentials more negative than –20 mV in Na^+-free, 10 mM Ca^{2+} solution ($n = 10$), indicating a high permeability to Ca^{2+} (the ratio of the permeability coefficients of Ca^{2+} and Cs^+, $P_{Ca}/P_{Cs} \approx 2.7$) (Fig. 2A, left). Two days after infection with the three recombinant viruses (AxCALNLGluR2, AxCAGFP, and AxCANCre), the degree of inward rectification was markedly attenuated in Bergmann glia emitting GFP. In 14 of 23 cells (61%), the *I-V* relation of AMPARs exhibited outward rectification, and AMPA elicited no inward current in Na^+-free, 10 mM Ca^{2+} solution at –80 mV, indicating negligible permeability to Ca^{2+} ($P_{Ca}/P_{Cs} < 0.17$) (Fig. 2A, right). To quantify the degree of rectification, we introduced the rectification index (RI), defined as the conductance of the AMPA response measured at +40 mV divided by the conductance at –60 mV (*14*). The RIs were <0.25 in all 21 cells without GluR2 expression (0.13 ± 0.02), and those in 23 cells with GluR2 expression ranged

[1]Gunma University School of Medicine, Maebashi, Gunma 371-8511, Japan. [2]Core Research for Evolutional Science and Technology, Japan Science and Technology Corporation, Kawaguchi, Saitama 332-0012, Japan. [3]Department of Neurobiology, Tokyo Metropolitan Institute for Neuroscience, Fuchu 183-8526, Japan. [4]Institute of Medical Science, University of Tokyo, Tokyo 108-0071, Japan.

*To whom correspondence should be addressed. E-mail: ozawas@med.gunma-u.ac.jp

from 0.64 to 1.44 (1.03 ± 0.05; $P < 0.0001$). Infection with AxCALALGluR2-IRES-GFP, together with AxCANCre, similarly increased the RIs. The RIs ranged from 0.54 to 1.19 (0.90 ± 0.07; $n = 11$) in Bergmann glial cells co-infected with these viruses, whereas those infected with AxCALALGluR2-IRES-GFP and AxCAGFP, but without AxCANCre, were <0.25 in all 11 cells (0.11 ± 0.02; $n = 11$). Figure 2B is a histogram showing the distribution of the RIs obtained from cells with and without GluR2 expression. Because the RI is correlated closely with the Ca^{2+} permeability (*15*), these results indicated that the Ca^{2+} permeability of AMPARs in Bergmann glia was efficiently reduced by the adenoviral-mediated transfer of GluR2 cDNA.

Bergmann glial cells have processes with arborized, irregularly shaped lamellate appendages that wrap synapses on Purkinje cell spines and seal the synaptic cleft almost completely (*16*). These characteristic features of the relation between Bergmann glial processes and Purkinje cell synapses were well preserved 2 to 4 days after infection with adenoviral vectors without GluR2 expression (Fig. 3, A and C) (*9*). In contrast, 2 days after viral infection for expression of GluR2, the morphology of the glial processes changed markedly. The arborized fine glial processes were retracted to form smooth ball-like structures, and the lamellate appendages were mostly lost (Fig. 3B). The fine lamellate structures of the glial processes were also lost 2 days after GluR2 expression (Fig. 3D). At this stage, most synapses on Purkinje cell dendritic spines were no longer ensheathed by the glial leaflet-like processes, and swellings of presynaptic nerve terminals were often detected in synapses without such glial ensheathing (Fig. 3D, inset) (*17*). Adenoviral-mediated overexpression of the GluR1 subunit induced no such morphological changes, indicating that these effects of GluR2 expression are not side effects related to overexpressing a GluR subunit.

Bergmann glial processes surrounding excitatory synapses on Purkinje cells express high levels of the glutamate transporter GLAST, which limits the duration of synaptic transmission by rapidly taking up released glutamate (*12, 18, 19*). Agents blocking the action of the glutamate transporter prolong the excitatory postsynaptic currents (EPSCs) in Purkinje cells (*20*). We therefore examined whether GluR2 expression in Bergmann glia affected synaptic transmission in parallel fiber (PF) and climbing fiber (CF) Purkinje cell synapses. We recorded from Purkinje cells surrounded by Bergmann glia emitting GFP in cerebellar slices infected with either the mixture of AxCALNLGluR2 plus AxCANCre plus AxCAGFP or that of AxCALALGluR2-IRES-GFP plus AxCANCre 2 days before the experiments. Control recordings were performed in slices infected with AxCALNLGluR2 (or AxCALALGluR2-IRES-GFP) plus AxCAGFP, without AxCANCre. Sample records of PF-mediated EPSCs (PF-EPSCs) in Purkinje cells in slices without and with GluR2 expression are shown in CTZ(–) traces in Fig. 4A, left and right, respectively. GluR2 expression significantly increased the decay time constant of the PF-EPSC from 11.8 ±

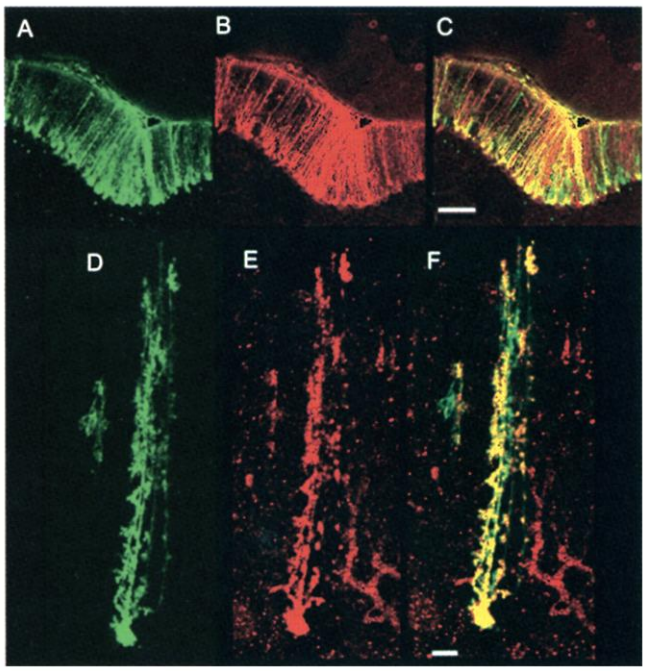

Fig. 1. Adenoviral-mediated expression of GFP and GluR2 in Bergmann glia. (**A** through **C**) A confocal section showing expression of GFP (A), GluR2 (B), and a merged image (C) in a 200-μm-thick slice that is infected with the viral mixture of AxCALNLGluR2 plus AxCANCre, together with AxCAGFP. (**D** through **F**) An example of coexpression of GFP (D) and GluR2 (E) in an isolated single Bergmann glia and a merged image (F). Scale bars represent 50 μm for (A) through (C) and 10 μm for (D) through (F).

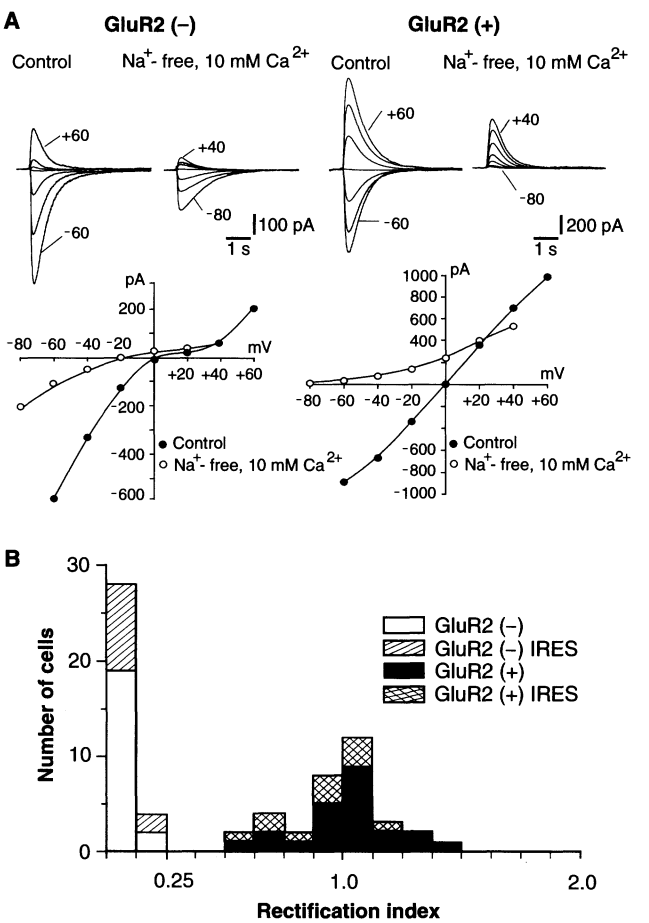

Fig. 2. Changes in electrophysiological properties of AMPA receptors caused by GluR2 expression in Bergmann glia. (**A**) Current responses to AMPA without (left) and with (right) GluR2 expression. AMPA responses were recorded at membrane potentials between −60 and +60 mV in a control solution and between −80 and +40 mV in a Na^+-free, 10 mM Ca^{2+} solution. In the graphs, the amplitude of the current response was plotted against the membrane potential. The external solution contained 50 μM CTZ. The current traces on the left [GluR2 (–)] were taken from a glia emitting GFP in slices infected with AxCALNLGluR2 plus AxCAGFP. (**B**) Histogram showing the distribution of the RI. The RIs were obtained from 23 cells infected with AxCALNLGluR2 plus AxCANCre plus AxCAGFP (solid columns) and 11 cells infected with AxCALALGluR2-IRES-GFP plus AxCANCre (double-hatched columns). As controls, they were obtained from 21 cells infected with AxCALNLGluR2 plus AxCAGFP (open columns) and 11 cells infected with AxCALALGluR2-IRES-GFP plus AxCAGFP (single-hatched columns).

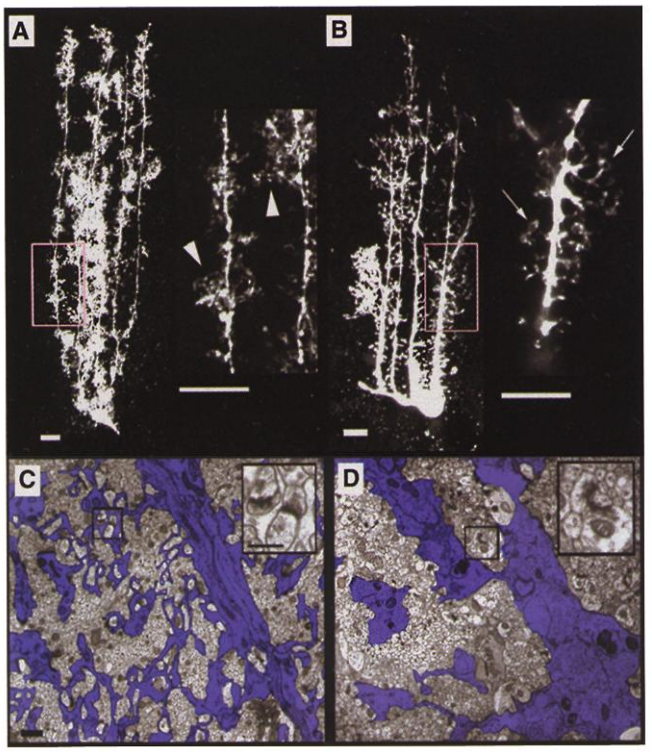

Fig. 3. Changes in morphology of glial processes caused by GluR2 expression. (**A**) Confocal image of a lucifer yellow–injected Bergmann glia without GluR2 expression. The cell was infected with AxCALALGluR2-IRES-GFP, but without AxCANCre. A minimum amount of AxCAGFP (3.0×10^5 PFU) was co-injected to mark inoculated cells. (**B**) Confocal image of a lucifer yellow–injected glia expressing GluR2. The cell was infected with AxCALALGluR2-IRES-GFP plus AxCANCre. Higher magnification of the boxed areas in (A) and (B) is shown on the right of each panel. Twenty serial optical sections of 3 and 1 μm are projected in the lower and higher magnification views, respectively. Arrowheads in (A) and arrows in (B) indicate lamellate appendages of the glial processes and their ball-like retraction, respectively. (**C** and **D**) Electron microscopy of the molecular layer of the cerebellar cortex infected with AxCALALGluR2-IRES-GFP plus AxCAGFP [GluR2 (–)] (C) and with AxCALALGluR2-IRES-GFP plus AxCANCre [GluR2 (+)] (D). Processes of Bergmann glia are false-colored blue. The insets show higher magnification views of the boxed areas. Scale bars represent 10 μm in (A) and (B), 1 μm in (C) and (D), and 0.5 μm in the insets of (C) and (D).

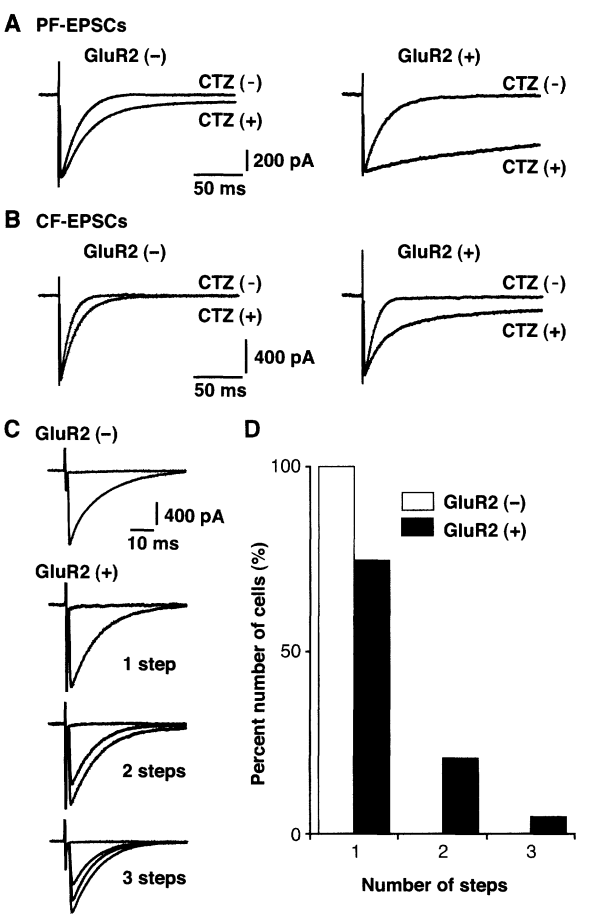

Fig. 4. Prolonged decay of EPSCs and multiple CF innervation of Purkinje cells after GluR2 expression in Bergmann glia. (**A**) PF-EPSCs in the absence and presence of 100 μM CTZ, without and with GluR2 expression. Peak amplitudes of the EPSCs in the presence of CTZ were normalized to those in the absence of CTZ. Each trace is the average of five consecutive EPSCs at –50 mV. (**B**) CF-EPSCs in the same arrangement as in (A), except that the holding potential was –10 mV. (**C**) All-or-none CF-EPSCs without GluR2 expression (top trace) and representative CF-EPSCs with one, two, or three discrete steps (lower three traces) after GluR2 expression. The holding potential was –10 mV. (**D**) Histogram showing the number of discrete steps of CF-EPSCs recorded in Purkinje cells in slices without (open column) and with (solid columns) GluR2 expression. Numbers of cells tested without and with GluR2 expression were 50 and 63, respectively.

0.9 ms (n = 14) to 18.8 ± 1.3 ms (n = 13) ($P <$ 0.001). This suggested that the removal of the synaptically released glutamate was retarded by GluR2 expression. Because the decay kinetics of the EPSC are at least partially affected by desensitization of the postsynaptic AMPARs (*20*), elimination of this desensitization by CTZ should reveal the impaired clearance of glutamate more clearly. We compared the decay kinetics of PF-EPSC with and without GluR2 expression in the presence of 100 μM CTZ. Under these conditions, the decay time constant was 30.6 ± 2.5 ms (n = 12) without GluR2 expression (Fig. 4A, left). After GluR2 expression, this value was increased to 478.0 ± 65.4 ms (n = 10) (Fig. 4A, right). Thus, clearance of synaptically released glutamate was retarded severely in the PF synapse by GluR2 expression in Bergmann glia.

For CF-mediated EPSCs (CF-EPSCs), the average decay time constants were 7.9 ± 0.5 ms (n = 11) and 8.2 ± 0.6 ms (n = 11), without and with GluR2 expression, respectively; the difference was not significant ($P > 0.58$). However, a clear difference was detected in the decay time course of EPSCs in the presence of 100 μM CTZ (Fig. 4B). Without GluR2 expression, application of 100 μM CTZ increased the decay time constant to 17.2 ± 2.2 ms (n = 12) (Fig. 4B, left). With GluR2 expression, CTZ prolonged the CF-EPSC more markedly (Fig. 4B, right). Under these conditions, the decay time course was fitted by two exponentials, the mean time constants being 21.2 ± 2.6 and 179.6 ± 46.2 ms, with the mean amplitude of the slower component making up 36.8 ± 5.4% of the total when extrapolated to the peak (n = 12). These results indicated that GluR2 expression in Bergmann glia also impaired the removal of synaptically released glutamate in the CF Purkinje cell synapse, although to a lesser extent than in the PF synapse.

The impaired uptake of glutamate in both PF and CF synapses is most likely due to the increase in the distance from these synapses to the glial membranes at which GLAST is located. However, the postsynaptic glutamate transporter expressed in Purkinje cells at high densities has been shown to take up glutamate (*21*). Therefore, the possibility is not excluded that GluR2 expression in Bergmann glia somehow lowers expression of the postsynaptic transporter in Purkinje cells, which would also be responsible for the impaired uptake of glutamate.

Finally, we found that ~25% of Purkinje cells (16 out of 63 cells) were innervated by two (in 13 cells) or three (in 3 cells) CFs after expression of GluR2 in Bergmann glia in 22- to 26-day-old rats (Fig. 4, C and D). The multiple innervation of Purkinje cells by CF in the rat cerebellum is known to be eliminated completely by postnatal day 15 (*22*) and was not seen in cerebellar slices infected with adenoviral vectors without GluR2 expression in 22- to 26-day-old rats (n = 50). Therefore, Ca^{2+}-permeable

AMPARs in Bergmann glia are necessary for preventing surplus CFs from producing synapses onto single Purkinje cells.

Conversion of Ca^{2+}-permeable AMPARs into Ca^{2+}-impermeable receptors in Bergmann glia elicited morphological changes in fine glial processes wrapping Purkinje cell synapses, prolonged the kinetics of glutamatergic synaptic transmission, and caused multiple innervation of Purkinje cells by CFs. Thus, the morphology of glial processes and the synaptic activities would be interdependent. The Ca^{2+}-permeable AMPARs in glial cells probably play key roles in such interactions between glia and glutamatergic synapses.

References and Notes

1. P. H. Seeburg, *Trends Neurosci.* **16**, 359 (1993).
2. M. Hollmann, S. Heinemann, *Annu. Rev. Neurosci.* **17**, 31 (1994).
3. C. Steinhauser, V. Gallo, *Trends Neurosci.* **19**, 339 (1996).
4. M. Hollmann, M. Hartley, S. Heinemann, *Science* **252**, 851 (1991).
5. N. Burnashev, H. Monyer, P. H. Seeburg, B. Sakmann, *Neuron* **8**, 189 (1992).
6. K. Keinänen *et al.*, *Science* **249**, 556 (1990).
7. T. Müller, T. Möller, T. Berger, J. Schnitzer, H. Kettenmann, *Science* **256**, 1563 (1992).
8. N. Burnashev *et al.*, *Science* **256**, 1566 (1992).
9. For the methods used, see the supplementary information on *Science* Online at www.sciencemag.org/cgi/content/full/292/5518/926/DC1.
10. K. A. Yamada, C. M. Tang, *J. Neurosci.* **13**, 3904 (1993).
11. K. M. Partin, M. W. Fleck, M. L. Mayer, *J. Neurosci.* **16**, 6634 (1996).
12. J. A. Dzubay, C. E. Jahr, *J. Neurosci.* **19**, 5265 (1999).
13. M. Iino, S. Ozawa, K. Tsuzuki, *J. Physiol.* **424**, 151 (1990).
14. S. Ozawa, M. Iino, K. Tsuzuki, *J. Neurophysiol.* **66**, 2 (1991).
15. T. Isa, S. Itazawa, M. Iino, K. Tsuzuki, S. Ozawa, *J. Physiol.* **491**, 719 (1996).
16. J. Grosche *et al.*, *Nature Neurosci.* **2**, 139 (1999).
17. Quantitative evaluation of the morphological changes is available in the supplementary information on *Science* Online at www.sciencemag.org/cgi/content/full/292/5518/926/DC1.
18. F. A. Chaudhry *et al.*, *Neuron* **15**, 711 (1995).
19. K. Yamada *et al.*, *J. Comp. Neurol.* **418**, 106 (2000).
20. B. Barbour, B. U. Keller, I. Llano, A. Marty, *Neuron* **12**, 1331 (1994).
21. C. Auger, D. Attwell, *Neuron* **28**, 547 (2000).
22. J. Mariani, J.-P. Changeux, *J. Neurosci.* **1**, 696 (1981).

8 January 2001; accepted 20 March 2001

Integrated Genomic and Proteomic Analyses of a Systematically Perturbed Metabolic Network

Trey Ideker,[1,2]* Vesteinn Thorsson,[1,2] Jeffrey A. Ranish,[1,2] Rowan Christmas,[1] Jeremy Buhler,[3] Jimmy K. Eng,[1] Roger Bumgarner,[4] David R. Goodlett,[1] Ruedi Aebersold,[1,2] Leroy Hood[1,2]

We demonstrate an integrated approach to build, test, and refine a model of a cellular pathway, in which perturbations to critical pathway components are analyzed using DNA microarrays, quantitative proteomics, and databases of known physical interactions. Using this approach, we identify 997 messenger RNAs responding to 20 systematic perturbations of the yeast galactose-utilization pathway, provide evidence that approximately 15 of 289 detected proteins are regulated posttranscriptionally, and identify explicit physical interactions governing the cellular response to each perturbation. We refine the model through further iterations of perturbation and global measurements, suggesting hypotheses about the regulation of galactose utilization and physical interactions between this and a variety of other metabolic pathways.

For organisms with fully sequenced genomes, DNA microarrays are an extremely powerful technology for measuring the mRNA expression responses of practically every gene (*1*). Technologies for globally and quantitatively measuring protein expression are also becoming feasible (*2*), and developments such as the two-hybrid system are enabling construction of a map of interactions among proteins (*3*). Although such large-scale data have proven invaluable for distinguishing cell types and biological states, new approaches are needed which, by integrating these diverse data types and assimilating them into biological models, can predict cellular behaviors that can be tested experimentally. We propose and apply one such strategy here, consisting of four distinct steps:

(i) Define all of the genes in the genome and the subset of genes, proteins, and other small molecules constituting the pathway of interest. If possible, define an initial model of the molecular interactions governing pathway function, drawn from previous genetic and biochemical research.

(ii) Perturb each pathway component through a series of genetic (e.g., gene deletions or overexpressions) or environmental (e.g., changes in growth conditions or temperature) manipulations. Detect and quantify the corresponding global cellular response to each perturbation with technologies for large-scale mRNA- and protein-expression measurement.

(iii) Integrate the observed mRNA and protein responses with the current, pathway-specific model and with the global network of protein-protein, protein-DNA, and other known physical interactions.

(iv) Formulate new hypotheses to explain

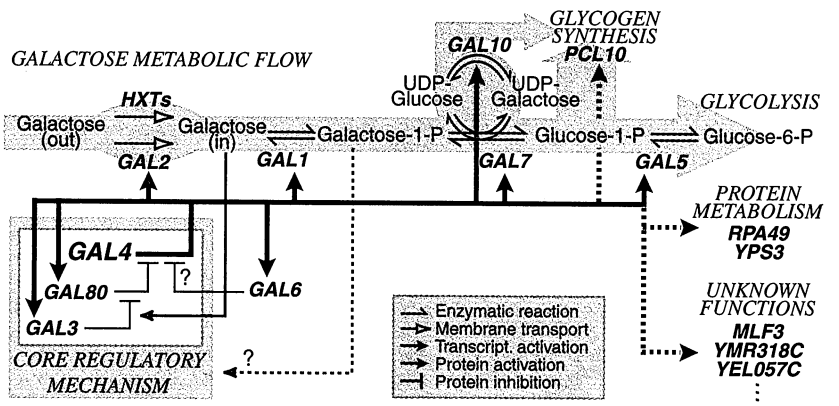

Fig. 1. Model of galactose utilization. Yeast metabolize galactose through a series of steps involving the *GAL2* transporter and enzymes produced by *GAL1*, *GAL7*, *GAL10*, and *GAL5*. These genes are transcriptionally regulated by a mechanism consisting primarily of *GAL4*, *GAL80*, and *GAL3*. *GAL6* produces another regulatory factor thought to repress the GAL enzymes in a manner similar to *GAL80*. Dotted interactions denote model refinements supported by this study.

[1]The Institute for Systems Biology, 4225 Roosevelt Way NE, Suite 200, Seattle, WA 98105, USA. Departments of [2]Molecular Biotechnology, [3]Computer Science, and [4]Microbiology, University of Washington, Seattle, WA 98195, USA.

*To whom correspondence should be addressed at The Institute for Systems Biology. E-mail: tideker@systemsbiology.org